ANALYSIS OF FIBER STEERING EFFECTS IN THERMOPLASTIC AUTOMATED FIBER PLACEMENT

Thomas Zenker[1] and Maximilian Schwab[1]

[1]Fraunhofer Research Institution for Casting, Composite and Processing Technology IGCV,
Am Technologiezentrum 2, 86159 Augsburg, Germany
Email: thomas.zenker@igcv.fraunhofer.de, web page: https://www.igcv.fraunhofer.de/en.html

Keywords: Automated Fiber Placement, thermoplastic, steering, MATLAB, undulations

Abstract
This paper investigates aspects of non-geodesic layup in Thermoplastic Automated Fiber Placement (TAFP). To study possible effects on process and layup quality, coupon laminates with curved fiber paths at variable radii were manufactured. Process parameters were varied systematically. The temperatures at the nip point were recorded with an infrared camera system and matched with the robot position data. The resulting temperature plots were used to analyze the temperature distribution, yielding particularities of steering layup regarding energy absorption behavior. Further, an optical sensor was used to record a raw image of the fiber angle distribution. A MATLAB routine was developed for detecting undulations, which were characterized in terms of wavelength. The routine was validated by microscopic analysis, and subsequently applied to analyze the fiber undulation distribution over a tow width. Finally, the trajectory radius and process parameters were correlated to the resulting undulations on tape level.

1. Introduction

Automated Fiber Placement (AFP) is one of the most promising manufacturing technologies for the highly automated production of complex CFRP-parts. Using the process as a preforming technique for unidirectional (UD-) tapes with thermoplastic matrix systems, high layup rates can be realized, especially in comparison to fiber placement with in-situ consolidation. The degrees of freedom of the robot based layup system offer unique possibilities to produce complex geometries in or near net-shape. This often requires the layup of non-geodesic paths, which is referred to as fiber steering. Thereto regarding the machine movements, the layup head needs to rotate around the z-axis when following such curved trajectories. Consequently, the material is bent in plane and therefore locally subjected to tensile and compressive stresses [1]. This can result in various effects such as fiber waviness, tow buckling or inhomogeneous temperature distribution.
Fiber steering has been investigated by several authors for thermoset prepreg and dry fiber placement. Many investigations in the field of steering aim at the determination of the material- and process-specific minimum steering radius and the correlations between process parameters and achievable layup quality [2–4]. Hörmann [4] studied the steering induced fiber waviness for thermoset AFP layup. A computational model for in-plane waviness prediction was proposed. Here, a differentiation between in-plane undulations, out of plane tow buckling and tow pull-off, as a result of the occurring mechanical deformations, was made. Other publications mention different classifications, e.g. tow buckling, tow pull-up and tow misalignments [5].
Different techniques were recently applied to characterize the fiber waviness in thermoset UD prepreg material. Sutcliffe et. al. [6] compare micrographs in combination with image processing routines to Micro-CT images for the purpose of analyzing in-plane and out-of-plane fiber waviness. Further methods apply eddy current sensor devices for the detection of in-plane as well as out-of-plane

undulations [7, 8]. In the field of dry fiber placement, Veldnez et. al. [9] use a laser scanner to find quantitative correlations of the steering radius and the extent of out-of-plane undulations.
TAFP process development and optimization in general is widely covered by numerous studies (e.g. [10–12]). However, only little attention is dedicated to non-geodesic TAFP. This study can be seen as a first approach to investigate specific, fiber steering induces effects for TAFP. Since precise temperature control is essential for the layup quality achieved in the process, the influence of non-geodesic layup paths on the temperature distribution is investigated in the first step. Additionally, an optical fiber sensor device is applied to characterize process-induced fiber waviness on preform level.

2. Experimental work

2.1 Materials

Pre-impregnated unidirectional composite tape material with polyamide 6 (PA6) matrix and unspecified continuous carbon fiber (CF) was supplied by Celanese in form of ¼”-tows for the purpose of this study (Celstran CFR-TP PA6 CF60).

2.2 Specimen preparation

All layup trials of this study were conducted on a state-of-the-art industrial robot based 8-tow AFP machine by Coriolis Composites. A Laserline LDF 6000-100 diode laser device working at near-infrared wavelength range ($\lambda = 950 – 1040$ nm) with a maximum power of 6 kW is used as a primary heat source. Specimens were laid on a flat aluminum tooling covered with a polyimide film (Kapton HN 200, $t = 50$ µm). The compaction force and layup speed were kept constant at 1000 N, respectively 0.08 m/s, for all specimens. As laser power levels, 582 W, 632 W and 682 W were defined.

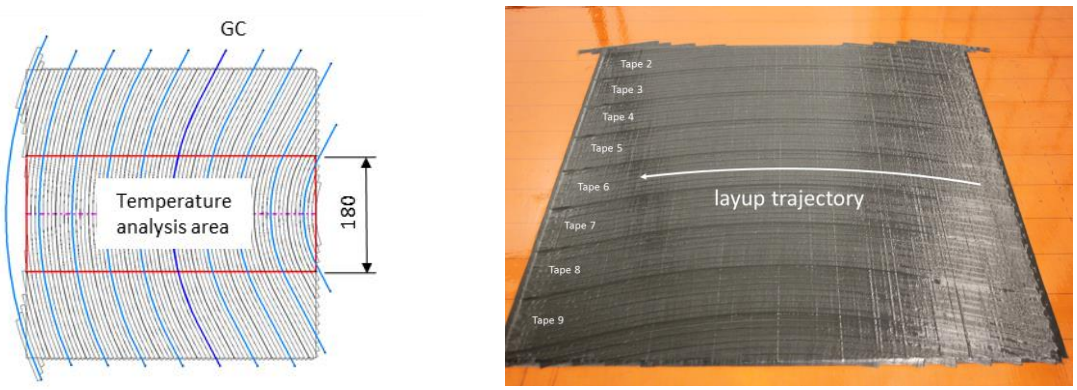

(a) (b)

Figure 1. (a) Specimen design, (b) r725-p632 specimen after layup

Fiber steering trials were examined on a [0/90]s substrate with dimensions of 350 x 350 mm, fabricated at constant processing parameters for all specimens. The guide curve (GC) of the steered paths was constructed symmetrically to the middle axis of the specimen (Figure 1 a). Specimens were manufactured with three different GC radii of 375 mm, 725 mm and 1075 mm. This initial GC was applied for the definition of tape 6 (Figure 1 b), all other tapes are generated based on parallels to this GC with an offset of 51.3 mm, which results in a nominal tape interval of 0.5 mm. This DoE yields a steering radius range from ~1200 mm to ~200 mm to be covered within this study.
Specimens are referred to according to their GC radius r and laserpower applied p. If a certain tape is considered, it is denoted as T, a certain tow as t.

2.3 Characterization

2.3.1 Temperature measurement

A FLIR 325sc infrared thermal camera was used to monitor the temperature during layup. As the camera works in the long wavelength infrared band (λ = 7.5 – 13.0 µm), no direct interference with the laser is expected. The camera has a resolution of approximately 0.72 mm at a working distance of ~500 mm. To determine the apparent emissivity of the material, a thermocouple based static calibration routine with an electrical hotplate as heat source was used. The calibration yielded an apparent emissivity of 0.95 for 160 °C.

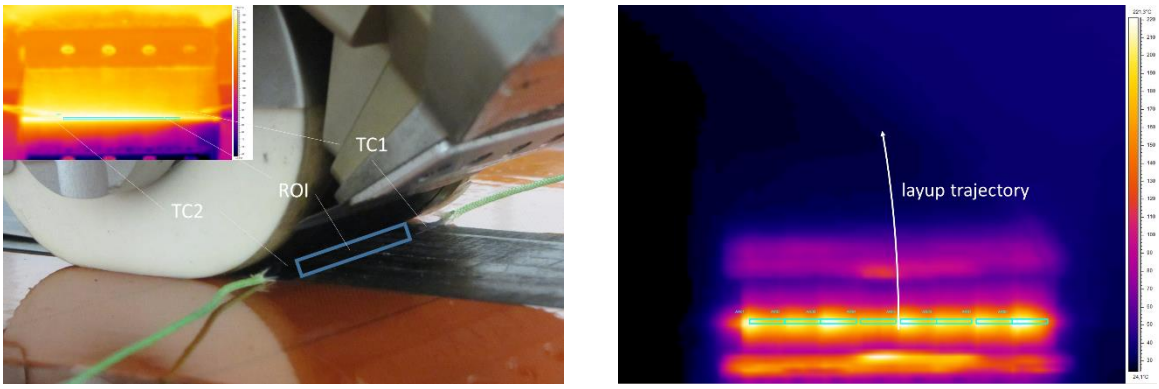

(a) (b)

Figure 2. (a) Emissivity calibration setup, (b) temperature analysis box definition

A Labview environment based recording routine was developed to enable the direct match of thermal and robot position data. For the analysis of tow discrete temperatures, independent analysis boxes with an array size of 9 x 2 pixels were defined for each tow (Figure 2 b). A vector based routine was implemented in VBA to calculate each tow's centerline position from the tool center point position data. The latter was recorded via the KUKA RSI interface. MATLAB was used to plot these sets of tow-fine data in form of a spatially resolved temperature map. For all numerical comparisons of the temperatures inside the steering area, an analysis area with length of 180 mm was defined symmetrically to the middle axis (Figure 1 a).

2.3.2 Equipment and methods for undulation characterization

For the characterization of in-plane undulations, a PROFACTOR FScan optical fiber angle sensor was used. The sensor uses a ring of 96 LEDs to generate illumination patterns of the specimen that are recorded with a CMOS camera at a resolution of 35 µm. Based on the principle of Photometric Stereo, these reflection patterns combined with a fiber reflection model yield different image modalities, among these the in-plane fiber orientation (azimuth angle). [13]
A MATLAB based routine was developed for the analysis of the sensor data (Figure 3). The original set of data is a 1600x1600 matrix of azimuth angles (α) related to the horizontal axis. In a first step, an algorithm is used to transform this data into angles relative to the local projection of the steered path's neutral fiber (α_r). Then, the analysis area is defined by user and data is cut accordingly. In a last transformation step, all data in this area is simplified to positive, negative and indifferent values to simplify the algorithm implementation and to increase visual comprehensibility. To counter possible misdetections, a defragmentation filter is applied before calculations were carried out. For validation of the algorithm, a Leica M80 stereo-microscope was used.

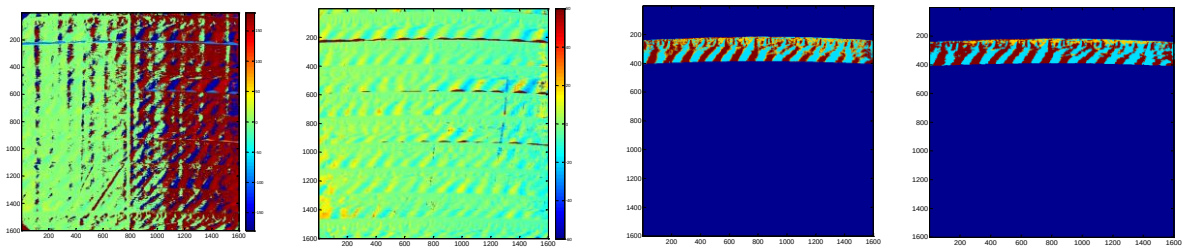

(a) (b) (c) (d)

Figure 3. (a) Original α matrix, (b) α_r matrix after angle transformation, (c) selected analysis area after tri-color tansformation, (d) selected tri-color area after defragmentation

For the assessment of the wavelength, the basic principle applied is to determine the spatial frequency of a wave, the wavenumber n, for each course of pixels inside a specified analysis area. This can be realized by creating the first derivative of the wave function and counting the present sign changes, which equals $n/2$. For the sensor data, this corresponds to a sign change of α_r, as illustrated in Figure 4.

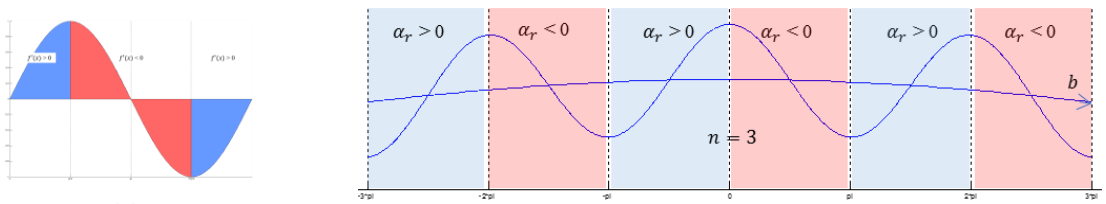

(a) (b)

Figure 4. (a) Areas with positive and negative derivation for f(x)=sin(x), (b) principle schematically applied on undulated fiber, n = 3

The wavelength λ is calculated as

$$\lambda = \frac{b}{n} \tag{1}$$

with the arc length b being taken from the chord s and circular height h by basic geometrical functions:

$$b = \frac{2 * \arcsin\left(\frac{4hs}{4h^2 + s^2}\right) * (4h^2 + s^2)}{8h} \tag{2}$$

3. Results and discussion

3.1 Temperature analysis

Figure 5 shows spatially resolved temperature maps of all three specimens manufactured at 682 W laser power. The presented temperature code ranges from 0 C to 460 °C. The average temperature increases with decreasing steering radius.

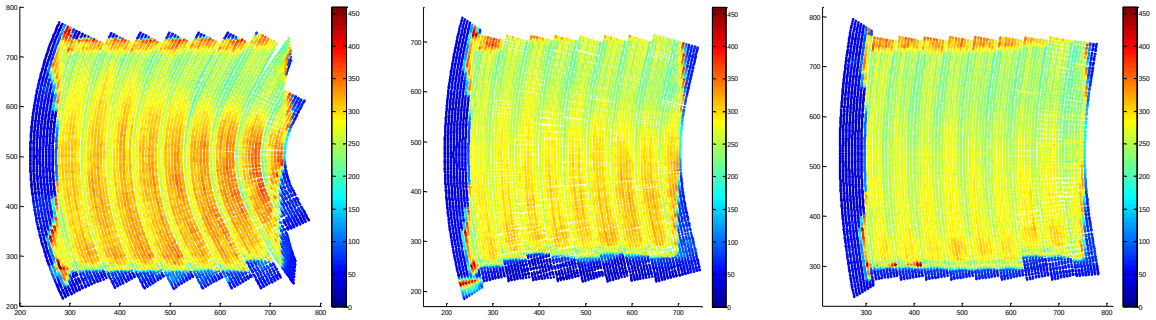

(a) (b) (c)

Figure 5. (a) Temperature map for specimen r375-p682, (b) r725-p682, (c) r1075-p682

This observation can be confirmed by Figure 6 (a), which presents the average course temperatures over the steering radius for all specimens under investigation. Further, Figure 6 (a) show that according to expectations an increased laser power leads to a higher average course temperature.

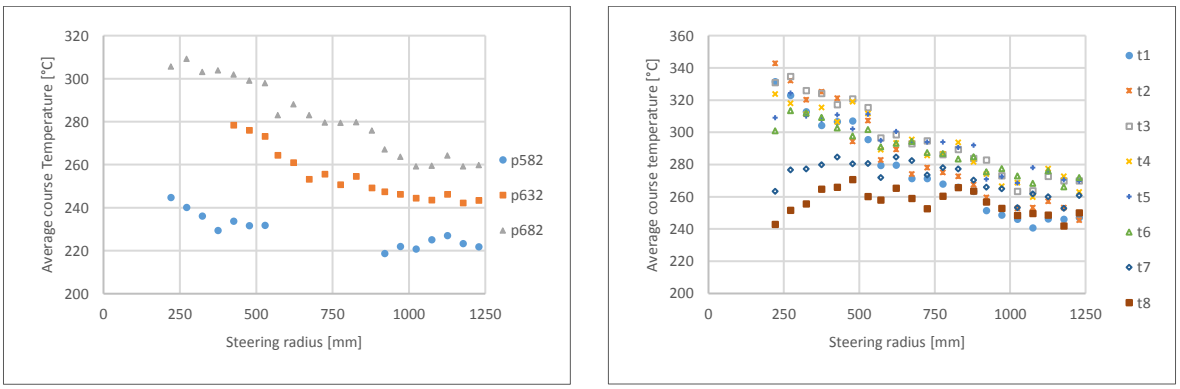

(a) (b)

Figure 6. (a) Tape-fine temperature over steering radius for varying laser powers, (b) tow-fine temperatures over steering radius for p682

Figure 6 (b) shows a tow-discrete average course temperature plot for all specimens manufactured at a laser power of 682 W. For steering radii > ~800 mm, the four tows in the center region of the compaction roller (t3 – t6) feature temperatures around 10 -25 K higher than the other tows. With reducing steering radius, temperatures shift in the way that tows on the outer side of the steered course show lower temperatures than tows on the inner side. This difference can be as high as ~100 K for a radius of ~220 mm. Possible explanations for these two phenomena can be found by fitting a line plot over roller width at different positions along the course is fitted with the caustic of the laser optics at the nip point (Figure 7 a). It can be noted that the laser energy density drops within the straight course area (approx. 6 mm from the course edge). This goes along with a temperature drop of the straight course (P3T5 plot) and could explain why the outer tows show less temperature at high steering radii, since they can be considered straight.

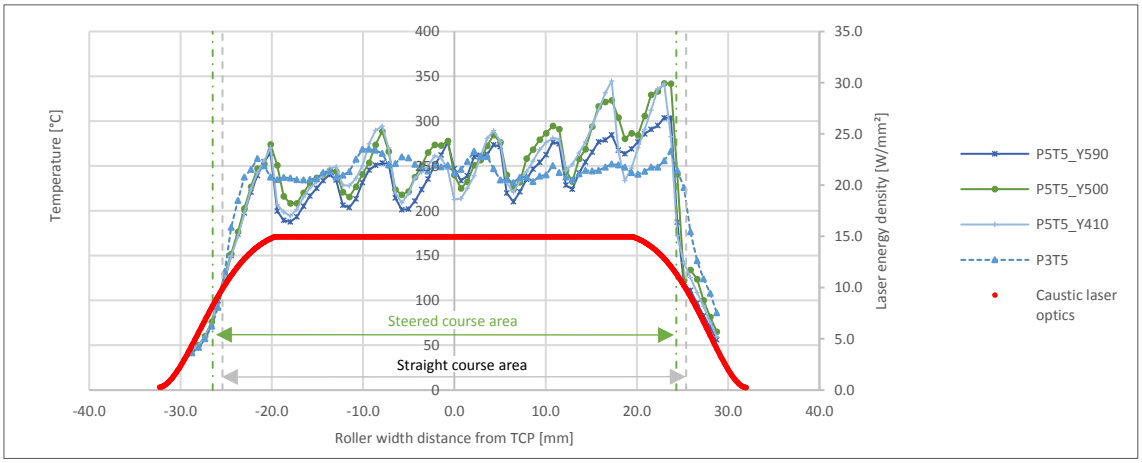

Figure 7. Temperature for selected courses of specimen r375-p582 and laser density over roller width

The three temperature plots of the steered courses (P5T5) show eight peaks over the course width, one for each tow. A possible explanation for these hotspots can be found in the study of the bending behavior of the tows between tow guidance and nip point during layup. As can be seen in Figure 8 (a), on the inner side of the curved path, tows loose contact to the roller, which equals a local thermal insulation from the heatsink (roller). Since these deformations get higher at lower steering radii, it is assumed that they are responsible for the previously described general increase of temperature with decreasing steering radius. Further, tows drift towards the outer side of the roller. Consequently, the inner tows move towards the area of maximum energy density.

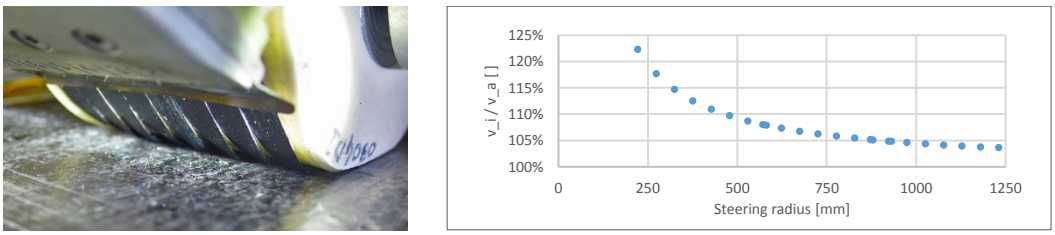

(a) (b)

Figure 8. (a) Tow bending during steered layup, (b) velocity gradient t1 to t8 as a function of the steering radius

Another reason for the thermal gradient over the roller width at low steering radius can be found in the layup kinematics of curved paths. Due to the rotational part of the head movement, the inner tows are placed at a higher velocity compared to the outer tows. This gradient increases exponentially with decreasing steering radius, as depicted in Figure 8 (b) for the relevant radii. As layup velocity is directly proportional to the amount of time that the material is exposed to laser radiation, energy absorption is affected by this kinematic phenomenon.

3.2 Undulation analysis

Figure 9 shows a fit of a microscopy image of p582-r725-T9-t2 with its MATLAB analysis output (tri-color image) and the corresponding plot of the calculated wavelengths over the distance from the outer tow edge. For this tow-fine analysis, it can be noted that high wavelengths >10 mm are observed on the outer tow edge area. This matches well with the straight fibers in this area, clearly seen in the microscopy image, and can be related to the tensile stress resulting from tow bending. On the inner side of the tow,

waves with a homogenous phase length and amplitude can be found in the microscopic image. These can be seen as result of the local compressive stress, the corresponding wavelength levels off at ~3 mm in this region.

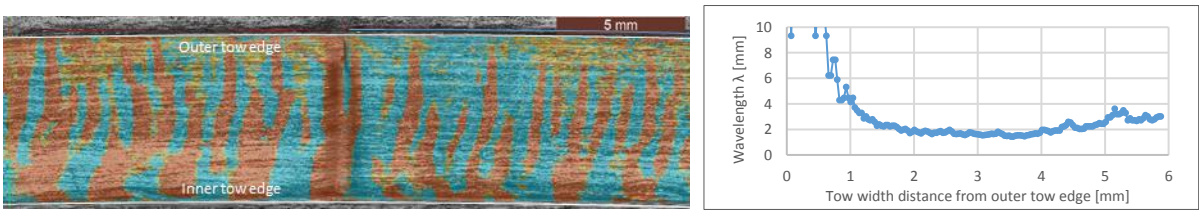

(a) (b)

Figure 9. (a) Fit of microscopic image and defragmented tri-color image r725-p582-T9-t2, (b) corresponding plot of wavelength over tow width distance

Regarding the fiber architecture transition from tensile to compressive region, it can be reported that straight fibers are only detected within a width of 1 mm from the outer tow edge. This means that the neutral axis moves towards the outer side of the tow during layup. This is due to a sudden stiffness reduction on the compressive side during layup when fibers start to undulate. Similar shifts of the neutral fiber have been reported e.g. for fiber microbuckling [14].
Figure 10 shows a plot of the wavelength over the roller width for a specimen tape with a nominal tape radius of 530 mm placed at 582 W laser power. For all eight tows, a peak at the tension side of the tow can be identified. However only a small region seems to be under tensile stress. After this peak, all tows show a trend of increasing wavelength towards the inner edge of the tow.

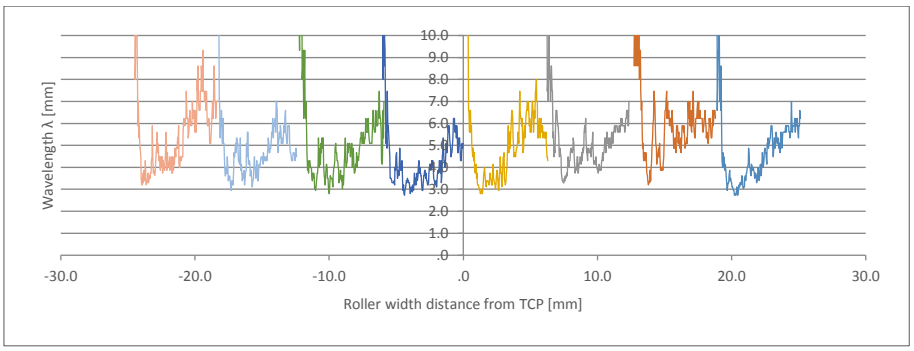

Figure 10. Wavelength over roller width for r725-p582-T3 (tape radius = 530 mm)

Since no significant differences between the tows could be identified, average values per tape were calculated to simplify the comparison of specimen manufactured at different laser power and various radii (Figure 11). For this comparison, only the half of the tow that was initially subject to compressive stress is considered.

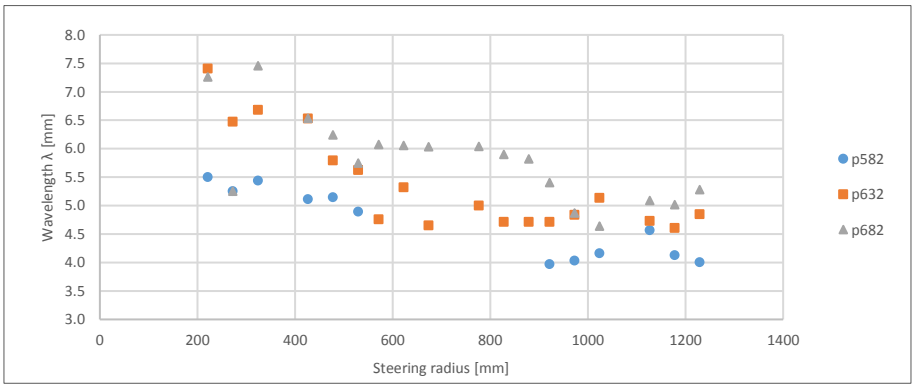

Figure 11. Average wavelength over steering radius for p582, p632 and p682 specimens

The tape-fine comparison shows an increasing wavelength with decreasing steering radius for all specimens. Alongside, for an equal radius, specimen manufactured at higher laser powers tend to show a higher wavelength compared to those manufactured at lower laser power. Both tendencies could be related to the decreasing viscosity of the PA6 matrix and UD-tape with increasing temperature ([15]), which could result in larger deformations at a certain load case. Furthermore, the increasing bending deflections with decreasing steering radius induces higher stress levels, which could also result in higher deformations.

3. Conclusions

An experimental study of the effects of non-geodesic TAFP layup was conducted. The analysis of the gathered IR camera data shows an increasing average temperature with decreasing steering radius on macroscopic level (tape-fine), which is possibly related to the thermal insulation of the tow due to bending induced deformation. Tow-fine analysis yields a temperature gradient over the roller width for small steering radii. This is attributed to steering induced tow deformation, tow drift and kinematic effects. These tendencies could be visualized well by a spatially resolved plot based on the robot position data.
To characterize in-plane undulations which occur due to tow bending, an optical fiber angle sensor was used. Based on the gathered images, a MATLAB algorithm was developed for wavelength calculation. Only a narrow tensile region with straight fibers was found on the outer edges of each tow, which indicates a shift of the neutral fiber in this direction.
Comparison of the average wavelength of the compression area shows an increasing wavelength for decreasing steering radius for a certain laser power as well as for higher laser powers. Both correlations could be linked to the reduced viscosity at higher processing temperatures. To fully characterize the wave patterns, a method to determine the corresponding amplitudes is currently being developed.
Since in-situ consolidation is currently not achievable for TAFP layup of such ambitious geometries, future work is required to study the behavior of the undulations in subsequent process steps. Mechanical characterization after consolidation of steered laminates could be the basis for the definition of application-specific knock-down factors for a certain degree of steering.

Acknowledgments

This work was financially supported by the Bavarian Ministry of Economic Affairs.
The authors acknowledge the assistance of Mr. Biali Lima Rodriguez for conducting parts of the wavelength analysis. Further, the authors want to thank the Chair of Carbon Composites, Technical University of Munich, for providing the PROFACTOR sensor equipment and the colleagues there for the fruitful technical discussions.

References

[1] A. W. Blom. *Structural performance of fiber-placed, variable-stiffness composite conical and cylindrical shells*. PhD thesis, Delft University of Technology, 2010.
[2] H. M. El-Dessouky, R. P. Smith, Z. Qureshi, and R. J. Scaife. Limitations of processing carbon fibre reinforced plastic/polymer material using automated fibre placement technology. *Journal of Reinforced Plastics and Composites*, 35:1527–1542, 2016.
[3] J. Chen *et al.* Impact of layup rate on the quality of fiber steering/cut-restart in automated fiber placement processes. *Science and Engineering of Composite Materials*, 22, 2015.
[4] P. Hörmann. *Thermoset automated fibre placement - on steering effects and their prediction*. PhD thesis, Technical University of Munich, Verlag Dr. Hut, 2016.
[5] D. H.-J.A. Lukaszewicz, C. Ward, and K. D. Potter. The engineering aspects of automated prepreg layup: History, present and future. *Composites Part B: Engineering*, 43:997–1009, 2012.
[6] M.P.F. Sutcliffe, S. L. Lemanski, and A. E. Scott. Measurement of fibre waviness in industrial composite components. *Composites Science and Technology*, 72:2016–2023, 2012.
[7] K. Mizukami, Y. Mizutani, A. Todoroki, and Y. Suzuki. Detection of in-plane and out-of-plane fiber waviness in unidirectional carbon fiber reinforced composites using eddy current testing. *Composites Part B: Engineering*, 86:84–94, 2016.
[8] A. Bouloudenine, M. Feliachi, and M. E. H. Latreche. Development of circular arrayed eddy current sensor for detecting fibers orientation and in-plane fiber waviness in unidirectional CFRP. *NDT & E International*, 92:30–37, 2017.
[9] L. Veldenz *et al.* Assessment of Steering Capability of Automated Dry Fibre Placement through a Quantitative Methodology. *Proceedings of the 3rd International Symposium on Automated Composites Manufacturing ACM-3, Montreal, Canada*, April 20 - 21 2017.
[10] W. J. B. Grouve, L. L. Warnet, B. Rietman, H. A. Visser, and R. Akkerman. Optimization of the tape placement process parameters for carbon–PPS composites. *Composites Part A: Applied Science and Manufacturing*, 50:44–53, 2013.
[11] C. M. Stokes-Griffin and P. Compston. The effect of processing temperature and placement rate on the short beam strength of carbon fibre-PEEK manufactured using a laser tape placement process. *Composites Part A: Applied Science and Manufacturing*, 78, 2015.
[12] A. Kollmannsberger, E. Ladstätter, and K. Drechsler. Challenges for thermoplastic-Automated Fiber Placement (TP-AFP) with in-situ consolidation on 3D parts. *Proceedings of the 17th European conference on Composite Materials ECCM-17, Munich, Germany*, June 26-30 2016.
[13] S. Zambal, W. Palfinger, M. Stöger, and C. Eitzinger. Accurate fibre orientation measurement for carbon fibre surfaces. *Pattern Recognition*, 48:3324–3332, 2015.
[14] T. Murphey, T. Meink, and M. Mikulas. Some micromechanics considerations of the folding of rigidizable composite materials. *Proceedings of the 19th Applied Aerodynamics Conference AIAA-19, Anaheim, USA*, June 11-14 2001.
[15] P. M. Schäfer. *Consolidation of carbon fiber reinforced polyamide 6 tapes using laser-assisted tape placement*. PhD thesis, Technical University of Munich, Verlag Dr. Hut, 2018.